An ultra-stable 2.9 μm guided-wave chip laser and application to nano-spectroscopy

D. G. Lancaster [ID], D. E. Otten [ID], A. Cernescu, N. Bourbeau Hébert, G. Y. Chen, C. M. Johnson [ID], T. M. Monro, and J. Genest

open access

View Online   Export Citation   CrossMark

ARTICLES YOU MAY BE INTERESTED IN

An ultra-stable 2.9 μm guided-wave chip laser and application to nano-spectroscopy

View Online   Export Citation   CrossMark

D. G. Lancaster,[1,2,a] (iD) D. E. Otten,[1,2] (iD) A. Cernescu,[3] N. Bourbeau Hébert,[4] G. Y. Chen,[1] C. M. Johnson,[5] (iD)
T. M. Monro,[1,6] and J. Genest[4]

AFFILIATIONS

[1] Laser Physics and Photonic Devices Laboratory, School of Engineering, University of South Australia, Mawson Lakes, 5095 SA, Australia
[2] Red Chip Photonics Pty Ltd, Mawson Lakes, 5095 SA, Australia
[3] NeaSpec GmBH, Munich-Haar D-85540, Germany
[4] Centre d'optique, Photonique et Laser, Université Laval, Québec City, Québec G1V 0A6, Canada
[5] Department of Chemistry, KTH, Royal Institute of Technology, Stockholm 10044, Sweden
[6] Defence Science and Technology Organisation, Department of Defence, Edinburgh, SA 5111, Australia

[a] david.lancaster@unisa.edu.au

ABSTRACT

We present a configurable guided-wave planar glass-chip laser that produces low-noise and high-quality continuous-wave laser emission tunable from 2.82 to 2.95 μm. The laser has a low threshold and intrinsic power and mode stability attributable to the high overlap of gain volume and pump mode defined by an ultrafast laser inscribed waveguide. The laser emission is single transverse-mode with a Gaussian spatial profile and $M^2_{x,y} \sim 1.05, 1.10$. The power drift is ~0.08% rms over ~2 h. When configured in a spectrally free-running cavity, the guided-wave laser emits up to 170 mW. The benefit of low-noise and stable wavelength emission of this hydroxide resonant laser is demonstrated by acquiring high signal-to-noise images and spectroscopy of a corroded copper surface film with corrosion products containing water and hydroxide ions with a scattering-scanning near-field optical microscope.

There is a scarcity of laser platform architectures in the mid-infrared (Mid-IR) spectral region, which limits the development of new photonic-based technologies. New emerging laser geometries such as optically pumped waveguide (WG) lasers[1,2] in the Mid-IR can motivate applications, with examples including atom trapping,[3] laser surgery,[4] and scattering-scanning near-field optical microscopy (s-SNOM), a technique to achieve nanospectroscopy of surfaces.[5] More generally, laser development in the 2.1–4 μm spectral region is immature, with very few application examples demonstrated using these lasers. Candidate technologies that will mature in the coming years include semiconductor, solid-state, and soft-glass fiber lasers.

It has recently been reported that type 1 interband cascade lasers (ICLs) can operate at room temperature, with continuous wave (CW) laser emission from a range of devices covering 1.9–3.3 μm.[6] There are still open issues regarding quantification of the beam-quality, mode stability,[7] and reliability. Low energy storage lifetimes and small mode volumes limit their suitability for high peak-power applications.

The development of mid-IR solid-state lasers has a long history and is dominated by 4-level erbium-doped bulk crystal lasers that can lase at discrete wavelengths across a "spiky" 2.7–2.9 μm crystal-field split (Stark dominated) transition.[8,9] These crystalline lasers are based on external cavity defined laser cavity modes, where the beam quality, divergence, and pointing stability are subject to the dynamics of thermal lensing, and the overlap of the pump and cavity modes. In addition, high thresholds due to large pump mode-volumes mean that water cooling of the laser crystal is typically implemented to control thermal lensing.

Transition metal Cr^{3+} doped ZnSe is an interesting evolving laser gain material, and recent work has reported improved optical quality that realizes the CW output in a bulk laser architecture achieving multi-watt-level performance and a tuning range of 1.9–3 μm.[10]

To improve the performance of such bulk material lasers, or even to achieve lasing, low-loss waveguides are required. For instance, rare-earth-doped fluorozirconate glass required a fiber geometry to lase,[11] but, in practice, such soft-glass fibers are fragile and difficult to manufacture. For low power applications, these challenges can be overcome when waveguide-in-bulk geometries were achieved,[12] enabled by ultrafast laser inscription (ULI) techniques.[13,14]

Ultrafast laser inscription (ULI) is a postprocessing technique that can be used to fabricate low-loss waveguides in bulk doped substrates.[15,16] By incorporating ULI waveguides in solid-state gain media, the laser threshold is reduced by the intrinsic overlap of the pump and cavity mode, with the added benefit of ensuring fundamental transverse-mode operation. These factors mean that ULI waveguides can allow lasing transitions in bulk gain materials that are generally not practical. For instance, another laser material that has benefitted from ULI waveguides is transition metal doped Cr:ZnSe planar waveguide lasers operating within 2–3 μm,[17] with waveguides greatly simplifying the required cavity designs.

In 2013, we reported first the operation of a Ho-doped fluorozirconate glass (ZrF_4, BaF_4, LaF_4, AlF_3, and NaF_3:ZBLAN) chip laser at ~2.9 μm.[18] However, its continuous-wave laser performance was marred by unstable pulsed emission as the population was "bottlenecking" in the Ho terminal $^5I_7$ laser level (μs pulses at 100–300 kHz). For reference, the HoPr energy levels are shown in Fig. 3(b). In this work, we report the elimination of bottlenecking for this 2.9 μm transition by addition of low concentration Pr^{3+} which provides a pathway to de-excite the Ho $^5I_7$ population, consistent with earlier work in HoPr ZBLAN fiber lasers.[19] Our motivation to demonstrate the improved continuous-wave (CW) performance from this 2.9 μm chip laser architecture is to set a foundation for further development toward mode-locking, Q-switching, and single-frequency operation.

This waveguide laser we report here exhibits noteworthy CW performance, with low power rms fluctuations of ~0.08% over 2 h in a grating stabilized cavity, and power up to 170 mW when configured in a contiguous cavity [described in Fig. 1(b)]. With a Littrow-configured diffraction grating, the laser is tunable from 2820 nm to 2950 nm. Beam quality is almost diffraction limited and symmetrical with $M^2_{x,y}$ ~ 1.05, 1.10. These near-ideal performance metrics are due to a combination of efficient optically pumped broadband gain near 2.9 μm, robust antireflection dielectric coatings on the chip, low-loss single-transverse-mode waveguides, and a simple and efficient cavity design. These characteristics are essential to meet the stringent requirements for long-term, maintenance-free precision applications. The wide and flat gain profile, as well as high upper state storage lifetimes (~3.2 ms[20]) of Ho^{3+} in ZBLAN glass, combined with large mode-area waveguides makes them promising candidates for high quality laser emission in mode-locking, single frequency, and Q-switching modes.
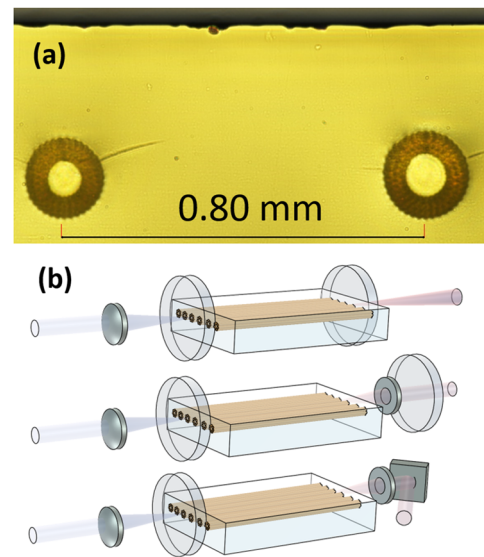

FIG. 1. (a) Bright-field microscope image of two waveguides (WGs) in the end facets of the chips. The waveguide centroids are ~350 μm below the surface, with the WG core diameter D_{left} ~ 80 μm and D_{right} ~ 100 μm. Claddings are ~55 μm thickness. (b) Cavity configurations reported in this paper. Cavity I is configured as a contiguous cavity with resonator mirrors "butted" to the gain chip; cavity II is an extended cavity; cavity III is an extended cavity with a diffraction grating configured in a Littrow geometry.

An application example is scanning near-field optical microscopy, and we present here high-resolution topographic and O–H absorption images of a copper film that has been corroded. For this nanospectroscopy demonstration, the chip laser is coupled to a neaSNOM (neaspec) near-field optical microscope.

The waveguides are fabricated in ingots of Ho, Pr codoped ZBLAN glass (2.5%, 0.25%, respectively). Depressed cladding waveguides are directly inscribed in the glass chips by ULI (5 MHz, <250 fs, and λ = 524 nm) produced from a frequency-doubled laser (IMRA, DE0210). Further details on the fabrication, morphology, and waveguide propagation loss (<0.3 dB/cm) of directly written waveguides in ZBLAN via ULI methods can be found in previously published work.[14,21,22]

In this work, we report the performance of an 18 mm long parallel polished chip that contains 6 waveguides with depressed claddings of 55 μm thickness, written with a range of core diameters sized between 60 and 100 μm. A bright-field microscope image of the transverse cross section of the waveguides is shown in Fig. 1(a). These "leaky-mode" waveguides are designed to preferentially guide fundamental-modes, and all waveguides were observed to operate in a lowest-order transverse mode for the range of cavity geometries shown in Fig. 1(b). Broadband antireflection coatings centered at 2.9 μm are applied to the chip facets (ion-beam sputtering) which also serve to protect the ZBLAN chip end-faces.

Individual waveguides are core-pumped by one or two polarization-combined single-mode fiber-coupled, polarization maintaining, 1155 nm diode lasers (Innolume GmbH). The maximum output of each pump laser is ~390 mW with the wavelength stabilized by fiber Bragg gratings. The pump output beam is coupled

to the waveguides via two BBAR coated relay lenses: a f = 8 mm molded aspheric lens to collimate the ferrule connector/angled physical contact (FC/APC) fiber output and a f = 40 mm aspheric lens to focus into the waveguide. The measured absorption of the HoPr codoped glass at 1155 nm is ~4 dB/cm.

Three laser cavity configurations are shown in Fig. 1. In all cases, the input coupler (IC) is a thin 12.7 mm diameter silica mirror designed to be a broad-band high-reflector (BBHR) from 2.7 to 3 μm, and highly transmitting (HT) at 1155 nm. The output coupler (OC) is either a 75% or 95% reflecting ZnSe 12.7 mm mirror (covering 2.7–3 μm) or a 450 grooves/mm 3.1 μm blazed diffraction grating (Thorlabs GR1325-45031) configured in a Littrow geometry. For the extended cavity (II), and the Littrow configured cavity (III), a f = 25 mm BBAR coated CaF$_2$ planoconvex lens is used to achieve cavity stability. When the cavity is aligned in a Littrow configuration, the grating is orientated to feed back the 1st order diffracted beam into the cavity axis. The 0th order provides output coupling. The reflectivity of the grating is specified at ~87% (~2.9 μm) for the polarization perpendicular to the grooves, thus indicating that the cavity will only reach the threshold for horizontally polarized light (orthogonal polarization is R ~ 24%).

The laser slope efficiency for a 18 mm long HoPr ZBLAN chip is shown in Fig. 2 for the three cavity configurations shown in Fig. 1. We note as well that no "cascade" emission near 2 μm was observed at any time, attributable to the $^5I_7$ terminal level population quenching by the Pr codopant.

Figure 2(a) shows the performance for the contiguous cavity with resonator mirrors (I) "butted-up" to the chip facets; either the R ~ 75% ($R_{75\%}$) or $R_{95\%}$ reflecting OCs are used, with a waveguide diameter of 100 μm. The measured slopes in Fig. 2(a) show a best slope efficiency for the $R_{75\%}$ OC ~ 21%, a $P_{threshold}$ of 104 mW, and

a maximum power of 170 mW (pump of 900 mW). Free-running wavelength is ~2870 nm, and quantum efficiency is 47%. The $R_{95\%}$ has a lower slope of ~15%, a lower $P_{threshold}$ of 39 mW.

Figure 2(b) shows slope efficiencies for the extended cavity configuration for the largest 100 μm diameter waveguide. Slopes of the $R_{75\%}$ and $R_{95\%}$ in extended cavity configuration are lower than in the contiguous cavity at 16% and 7%, respectively. The lower slope efficiency is attributed to a modal mismatch between the fundamental cavity transverse mode and the waveguide mode, thus leading to diffractive and coupling loss at the waveguide-air interface.

To demonstrate the tunability of this transition, a simple Littrow cavity is used (Fig. 1, cavity III). This cavity is pumped by a single pump diode laser operating at 350 mW (to reduce thermal loading on the passively cooled baseplate) and placed into a laser housing to further isolate the cavity from the open environment. The diffraction grating is held in a kinematic mount, thus allowing the grating angle and 1st order diffracted light, to be adjusted via rotating an 80 threads/in. screw. A consideration for the Littrow configuration is that the output beam angle (0th order) changes with grating angle. The slope efficiency/threshold for the Littrow configured cavity is consistent with the $R_{95\%}$ OC extended cavity, which likely indicates that the 1st order reflectivity is of similar magnitude. The laser threshold for the Littrow configured cavity is ~70 mW.

Figure 3 shows the measured tuning range of the laser when pumped by the single 350 mW pump diode. The maximum output power is 20 mW, and the spectral range achieved is ~128 nm, with range defined by 1 mW of power at the edges of the tuning curve and covering 2820–2948 nm. The emission has multiple longitudinal modes with a typical spectral width of ~0.25 nm (0.3 cm^{-1} or ~9 GHz). The cavity length is 85 mm, corresponding to a longitudinal mode spacing of ~1.6 GHz.

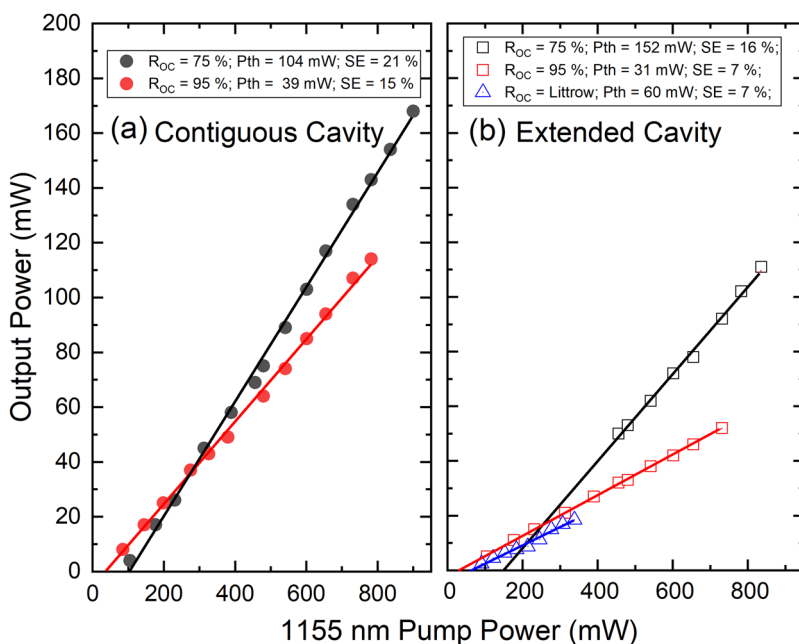**FIG. 2**. Continuous wave laser output of the L = 18 mm Pr-Ho-ZBLAN chip based laser. (a) Contiguous cavity operation where the mirrors are butted to the chip, and a 50 μm diameter WG is used. (b) Extended cavity operation with an intracavity lens for cavity stability and extended cavity operation with a 450 lines/mm diffraction grating configured in a Littrow configuration (blazed at 3.1 μm).
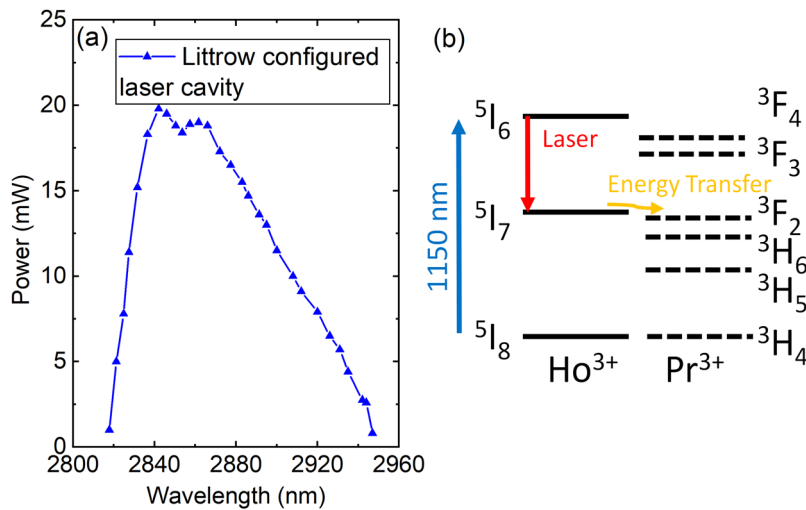
FIG. 3. (a) Measured tuning range of the Littrow configured chip laser for a pump power of 350 mW. (b) Energy level diagram for Pr Ho codoped ZBLAN.

The beam quality is observed to be consistent with a Gaussian shape. Beam quality was quantified by measuring the M^2 of the emission from the Littrow configured cavity (Fig. 4). A standard M^2 parameter is determined by fitting a hyperbolic curve to the beam diameter as a function of distance to the focus of the beam (the same method as in Ref. 23). To focus the beam, a BBAR coated CaF_2 f = 200 mm planoconvex lens is used, and the beam spatial shape was recorded by a Spiricon Pyrocam IV (Ophir). 2D Gaussian line shapes are fitted to the beam diameters to determine $1/e^2$, consistent with a second moment method ($D_4\sigma$). Beam quality is found to be close to symmetrical and measured at $M^2 \sim 1.10$ in the vertical dimension and $M^2 \sim 1.04$ in the horizontal plane.
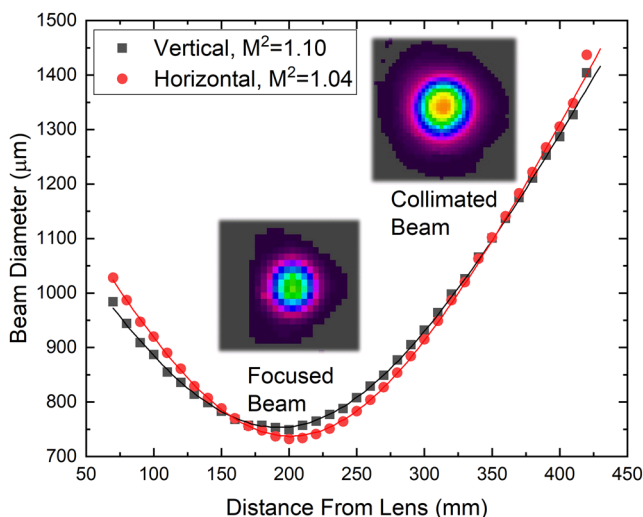
Stable output power is a desirable characteristic of a continuous-wave laser with clear benefits for applications such as spectroscopy and microscopy. To quantify the stability and drift of the CW emission, the Littrow configured laser (which is contained in a housing) is warmed up for 1 h and the power recorded every second for 2.3 h (Thorlabs PM100 + S401C thermal power head; 1.1 s time constant and 1 μW resolution). Laser power as a function of time is presented in the inset of Fig. 5, with the laser displaying an average power of ~14.1 mW, with a root mean square stability of ~±0.08%. We speculate that this high stability power output of this passively cooled laser can be partially attributed to the intrinsic modal overlap of the single transverse mode pump laser. In contrast, bulk solid-state lasers use multimode pump diodes due to increased mode-area and have imperfect overlap with the cavity-mode due to the thermal-lensing defined cavity-mode.

The relative intensity noise (RIN) of the laser emission was measured by use of a DC coupled amplified MCT detector (Vigo PVI-2TE-4; 50 MHz bandwidth) and is shown in Fig. 5. In our previous work,[18] the Ho doped laser pulsed at 100–300 kHz due to population bottlenecking in the terminal level lifetime (relaxation oscillation driven). The addition of Pr^{3+} serves to reduce the lower state lifetime, as evidenced by the absence of pulsed emission, or lasing from the $^5I_7$ terminal level. The RIN shows characteristic low-frequency mechanical noise (<200 Hz) and the relaxation oscillation at ~215 kHz. The RIN baseline is expected to decrease if operated as a single longitudinal laser as we estimate there are >5 longitudinal modes in the spectral output, leading to longitudinal mode competition.

An example of the use of the Ho chip laser is a study of the nanoscale distribution of water and hydroxide ions in a film of corrosion products on copper. A polished copper surface protected by octadecylphosphonic acid (ODPA, Sigma) was exposed to 80% RH and 100 ppb formic acid for 120 h to mimic the conditions for indoor atmospheric corrosion. The infrared reflection/absorption spectrum (IRRAS) with 1024 scans and 4 cm^{-1} resolution in Fig. 6 shows the formation of the corrosion products: copper formate at ~2800 cm^{-1}, imbedded water and hydroxide ions in the region ~2700–3600 cm^{-1},

FIG. 4. Measured beam-quality of the Littrow configured chip laser. Beam diameters are measured by a $D_4\sigma$ fit at each beam image. The beam is focused by a f = 200 mm CaF_2 lens, and beam images are recorded with a pyroelectric array camera.
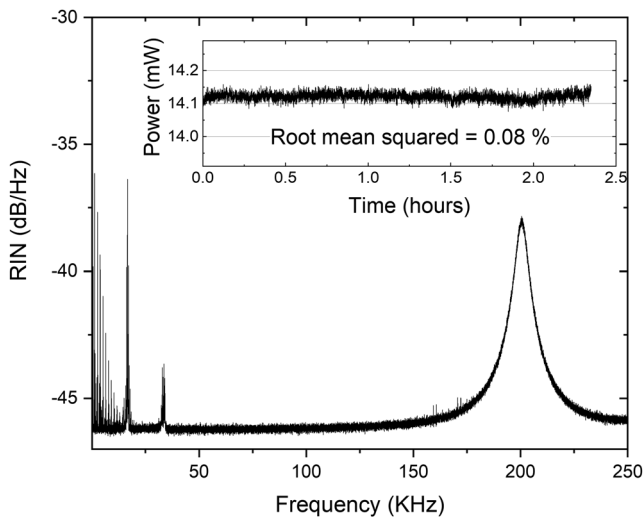
FIG. 5. The measured Relative Intensity Noise (RIN) of the Littrow configured chip laser with clear evidence of relaxation oscillations centered at ~203 kHz (300 mW pump). Inset: measured power stability of the Littrow configured chip laser after a 1 h warmup (1 s/measurement). The power stability is estimated by the root mean squared value of 0.08%.

FIG. 7. A false color image of the sample absorption (imaginary part of the s-SNOM signal) acquired by neaSNOM equipped with the Ho^{3+} chip laser tuned to 2900 nm. The image was collected in 231 s (6.6 ms integration/pixel). The red corresponds to strongest O–H absorption.

and nonhydrogen bonded OH groups in $Cu(OH)_2$ at 3570 cm^{-1}.[24] The spectrum is an average of an area larger than 1 cm^2 and does not provide important details on the spatial distribution of corrosion products.

In order to map the heterogeneity of the corrosion over a surface, the sample was imaged using neaSNOM—a commercial scattering near field optical microscope from neaspec—equipped with a Ho chip laser prototype built in partnership with Red Chip Photonics. A unique pseudoheterodyne detection technique used in neaSNOM allows for background-free measurements of reflectivity and most importantly absorption with nanoscale spatial resolution. Thus, tuning the laser emission to 3450 cm^{-1}, as indicated by the vertical dashed line in Fig. 6, allowed for nanoscale mapping of the distribution of water and hydroxide ions.
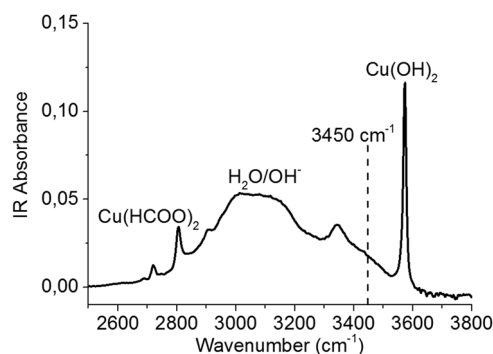
Figure 7 shows a high-contrast absorption map of a corroded sample area (4×3.5 μm^2) with 20 nm spatial resolution collected in less than 4 min. The map indicates a highly inhomogeneous distribution of the corrosion products and could be utilized for analysis of corrosion processes and their prevention.[25] Figure 8 shows an AFM topography image acquired simultaneously with the absorption map.

Notably, the low drift and low noise of the CW laser in combination with a high-stability neaSNOM microscope resulted in the uniform contrast in the absorption image.

In conclusion, our results verify that the ~2.9 μm CW laser performance of a holmium doped ZBLAN waveguide chip is substantially improved with the addition of a Pr codopant. The Pr reduces the $^5I_7$ terminal laser level lifetime, evidenced by results showing low-drift and ultrastable and low-noise CW emission in an external grating stabilized cavity configuration.

FIG. 6. An infrared reflectance/absorption spectrum of the corroded copper surface showing the different corrosion products formed. The vertical line shows the wavenumber (3450 cm^{-1}) at which the chemical mapping using neaSNOM equipped with the Ho chip laser was performed.
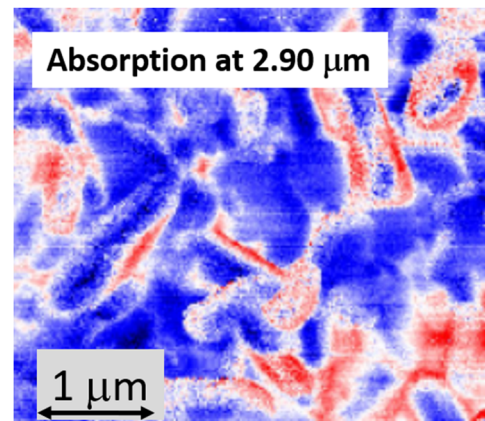

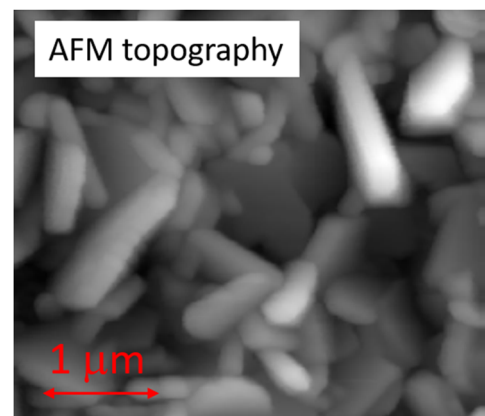**FIG. 8**. AFM topography image of a Cu formate sample surface. Image size is 4×3.5 μm^2.

Laser slope efficiencies of up to 21% for a contiguous cavity and 16% for an extended cavity were demonstrated; the maximum power at 2.9 μm of 170 mW and a tuning range of 2820 nm–2948 nm were also reported. Practical application of this ultrastable and passively cooled laser is demonstrated by using the tunable Ho chip laser to acquire high-resolution absorption imagery in a scanning near-field optical microscope (~20 nm resolution). A further favorable feature for long-term stable operation in an application such as nanospectroscopy is the intrinsic mode and pointing stability due to the waveguide in the gain chip.

REFERENCES

[1]C. Grivas, "Optically pumped planar waveguide lasers, Part I: Fundamentals and fabrication techniques," Prog. Quantum Electron. **35**(6), 159–239 (2011).

[2]C. Grivas, "Optically pumped planar waveguide lasers, Part II: Gain media, laser systems, and applications," Prog. Quantum Electron. **45-46**, 3–160 (2016).

[3]P. G. Mickelson, Y. N. Martinez de Escobar, P. Anzel, B. J. De Salvo, S. B. Nagel, A. J. Traverso, M. Yan, and T. C. Killian, "Repumping and spectroscopy of laser-cooled Sr atoms using the $(5s5p)^3P_2$–$(5s4d)^3D_2$ transition," J. Phys. B **42**, 235001 (2009).

[4]D. Chuchumishev, E. Nagel, A. Nierlich, S. Philipov, T. Genadiev, T. Fiebig, I. Buchvarov, and C.-P. Richter, "Mid-IR laser tissue ablation with little collateral damage using a laser tunable in the water absorption peak," in *2014 Conference on Lasers and Electro-Optics (CLEO) - Laser Science to Photonic Applications* (Optical Society of America, San Jose, CA, 2014), pp. 1–2.

[5]R. Krutokhvostov, A. A. Govyadinov, J. M. Stiegler, F. Huth, A. Chuvilin, P. S. Carney, and R. Hillenbrand, "Enhanced resolution in subsurface near-field optical microscopy," Opt. Express **20**, 593 (2011).

[6]M. Wang, T. Hosoda, J. Jiang, L. Shterengas, G. Kipshidze, A. Stein, T. Feng, and G. Belenky, "External cavity type-I quantum well cascade diode lasers with a tuning range of 440 nm near 3 μm," Opt. Lett. **43**, 4473–4476 (2018).

[7]L. Shterengas, G. Kipshidze, T. Hosoda, R. Liang, T. Feng, M. Wang, A. Stein, and G. Belenky, "Cascade pumping of 1.9–3.3 μm type-I quantum well GaSb-based diode lasers," IEEE J. Sel. Top. Quantum Electron. **23**(6), 1–8 (2017).

[8]H. Kawase and R. Yasuhara, "2.92-μm high-efficiency continuous-wave laser operation of diode-pumped Er:YAP crystal at room temperature," Opt. Express **27**(9), 12213–12220 (2019).

[9]W. Ma, L. Su, X. Xu, J. Wang, D. Jiang, L. Zheng, J. Liu, X. Fan, J. Liu, and J. Xu, "Improved 2.79 μm continuous-wave laser performance from a diode-end pumped Er,Pr:CaF_2 crystal," J. Alloys Compd. **695**, 3370–3375 (2017).

[10]S. B. Mirov, V. V. Fedorov, D. Martyshkin, I. S. Moskalev, M. Mirov, and S. Vasilyev, "Progress in mid-IR lasers based on Cr and Fe-doped II-VI chalcogenides," IEEE J. Sel. Top. Quantum Electron. **21**, 1 (2015).

[11]X. Zhu and N. Peyghambarian, "High power ZBLAN fiber lasers: Review and prospect," Adv. Optoelectron. **2010**, 501956.

[12]D. G. Lancaster, S. Gross, H. Ebendorff-Heidepriem, K. Kuan, T. M. Monro, M. Ams, A. Fuerbach, and M. J. Withford, "Fifty percent internal slope efficiency femtosecond direct-written Tm^{3+}:ZBLAN waveguide laser," Opt. Lett. **36**, 1587–1589 (2011).

[13]D. Choudhury, J. R. Macdonald, and A. K. Kar, "Ultrafast laser inscription: Perspectives on future integrated applications," Laser Photonics Rev. **8**, 827 (2014).

[14]S. Gross, M. Ams, G. Palmer, C. T. Miese, R. J. Williams, G. D. Marshall, A. Fuerbach, M. J. Withford, D. G. Lancaster, and H. Ebendorff-Heidepriem, "Ultrafast laser inscription in soft glasses: A comparative study of athermal and thermal processing regimes for guided wave optics," Int. J. Appl. Glass Sci. **3**, 332–348 (2012).

[15]K. M. Davis, K. Miura, N. Sugimoto, and K. Hirao, "Writing waveguides in glass with a femtosecond laser," Opt. Lett. **21**, 1729–1731 (1996).

[16]M. Ams, G. D. Marshall, P. Dekker, J. A. Piper, and M. J. Withford, "Ultrafast laser written active devices," Laser Photonics Rev. **3**, 535–544 (2009).

[17]J. R. Macdonald, S. J. Beecher, A. Lancaster, P. A. Berry, K. L. Schepler, and A. K. Kar, "Ultrabroad mid-infrared tunable Cr:ZnSe channel waveguide laser," IEEE J. Sel. Top. Quantum Electron. **21**, 375–379 (2015).

[18]D. G. Lancaster, S. Gross, H. Ebendorff-Heidepriem, M. J. Withford, T. M. Monro, and S. D. Jackson, "Efficient 2.9 μm fluorozirconate glass waveguide chip laser," Opt. Lett. **38**(14), 2588–2591 (2013).

[19]S. D. Jackson, "Single-transverse-mode 2.5-W holmium-doped fluoride fiber laser operating at 2.86 μm," Opt. Lett. **29**, 334–336 (2004).

[20]M. Kowalska, G. Klocek, R. Piramidowicz, and M. Malinowski, "Ultra-violet emission in Ho:ZBLAN fiber," J. Alloy Comput. **380**(1-2), 156–158 (2004).

[21]S. Gross, D. G. Lancaster, H. Ebendorff-Heidepriem, T. M. Monro, A. Fuerbach, and M. Withford, "Femtosecond laser induced structural changes in fluorozirconate glass," Opt. Mater. Express **3**(5), 574–583 (2013).

[22]F. Piantedosi, G. Y. Chen, T. M. Monro, and D. G. Lancaster, "Widely tunable, high slope efficiency waveguide lasers in a Yb-doped glass chip operating at 1 μm," Opt. Lett. **43**, 1902–1905 (2018).

[23]C. Khurmi, S. Thoday, T. M. Monro, G. Chen, and D. G. Lancaster, "Visible laser emission from a praseodymium-doped fluorozirconate guided-wave chip," Opt. Lett. **42**, 3339–3342 (2017).

[24]S. Hosseinpour, C. M. Johnson, and C. Leygraf, "Alkanethiols as inhibitors for the atmospheric corrosion of copper induced by formic acid: Effect of chain length," J. Electrochem. Soc. **160**, C270 (2013).

[25]C. M. Johnson and M. Böhmler, "Nano-FTIR microscopy and spectroscopy studies of atmospheric corrosion with a spatial resolution of 20 nm," Corros. Sci. **108**, 60–65 (2016).